

Cite this: DOI: 10.1039/c2jm00027j

www.rsc.org/materials

PAPER

## Patterned growth of vertically-aligned ZnO nanorods on a flexible platform for feasible transparent and conformable electronics applications

W. L. Ong,<sup>a</sup> Q. X. Low,<sup>b</sup> W. Huang,<sup>b</sup> J. A. van Kan<sup>c</sup> and G. W. Ho<sup>\*a</sup>

Received 3rd January 2012, Accepted 1st March 2012

DOI: 10.1039/c2jm00027j

Despite the attractiveness of low temperature hydrothermal processes, the synthesis of vertical ZnO nanostructures has mostly been limited to rigid substrates. Moreover, patterned growth of nanostructures is also commonly carried out on rigid substrates, since conventional optical lithography is not easily applied to polymeric substrates, as focusing and reaction of the substrate with the organic solvent used in the lithography process prove to be a challenge. Here, we demonstrate the limited work on laser writing lithography patterned growth instead of the commonly used soft lithography patterned growth of nanorods on the transparent flexible substrate polyethylene terephthalate (PET) with a practical device demonstration. The visibly-transparent nanorods on the PET platform constitute a superior structural integrity with ohmic electro-conductivity even in a highly bent state. Accordingly, this can pave the way towards integration of vertically-aligned 1D nanostructures on a flexible platform for a transparent, conformable, shock-proof and lightweight product.

### 1. Introduction

The development of high performance transparent and conformal electronic devices is one of the important research focus points, in view of the limitations of silicon-based electronics and the proliferation of portable display, communication, identification and various state-of-the-art electronics products. The accessibility to an optically transparent and mechanically flexible electronics platform is the essence of the next-generation display technologies, including other 'see-through' and conformable devices.

Polymer films are used as flexible substrates and are well-suited for conformal and highly transparent displays and organic electronic devices. Compared with the rigid and expensive substrates like silicon, sapphire *etc.*, a polymer has the inherent advantages of being light, flexible, cheap, and transparent. Among the various available polymer substrates, PET film has been widely used as a substrate for various kinds of devices, due to its transparency, flexibility, thermal resistance and mechanical strength. A single crystal ZnO nanowire field effect transistor (FET) was fabricated on a flexible PET substrate.<sup>1</sup> Ju *et al.* have also reported a transparent ZnO nanowire thin film transistor on a PET substrate of high electrical performance and optical transparency.<sup>2</sup> Other reported polymer substrates include a complementary inverter using n-channel sputtered ZnO and

p-channel pentacene channels on a polyethersulfone flexible substrate.<sup>3</sup>

Meanwhile, despite the merits of the hydrothermal approach, such as solution based, low temperature process and low fabrication costs, demonstrations of vertical ZnO nanostructures synthesis have been mostly limited to rigid and brittle substrates.<sup>4–6</sup> Vertically aligned ZnO nanostructure arrays are expected to show better performance than disordered nanostructures because of their optimized electrical pathways.<sup>6,7</sup> Other than the alignment of the nanowires, there have also been attempts to arrange them in regular patterns to further enhance device performance. The patterning of the nanowires on the substrate can be controlled by various techniques including optical lithography, soft lithography *etc.* However, conventional optical lithography patterning of nanostructures is commonly carried out on rigid substrates, since it cannot be easily applied to a polymeric substrate. For the case of optical lithography, the challenges lie in the focusing of light on a transparent and non-rigid substrate, and the reactivity of the polymeric substrate towards the organic solvent used in the lithography process. Accordingly, the integration of vertically aligned nanostructures with patterned/selective growth on a flexible platform for a transparent, conformable, shock-proof and lightweight product is a technological challenge.

There are reported works that demonstrate patterning of micro/nanostructures on flexible substrates mainly through soft lithography *e.g.* microcontact and nanoimprinting.<sup>8–10</sup> Kang *et al.* and Wang *et al.* have presented patterned growth of ZnO nanorods that combines the direct patterning of ZnO nanoparticle seeds *via* microcontact printing on flexible PET and Si substrates respectively. A semitransparent nanomesh Cu

<sup>a</sup>Department of Electrical and Computer Engineering, National University of Singapore, Singapore 117576, Singapore. E-mail: elehgw@nus.edu.sg

<sup>b</sup>Engineering Science Programme, National University of Singapore, Singapore 117576, Singapore

<sup>c</sup>Department of Physics, National University of Singapore, Singapore 117542, Singapore

electrode on a PET substrate, using metal transfer from a polydimethylsiloxane (PDMS) stamp based on nanoimprint lithography of specific pressure and temperature, is reported.

Although the soft lithography patterning of nanostructures on flexible substrates has been demonstrated, to the best of our knowledge there is limited work reported on laser writing based lithography towards patterned growth of nanorods on flexible substrates (PET). Thus, in this work, we present laser patterned growth of ZnO nanorods on flexible PET substrates. The visibly-transparent nanorods on the PET substrate constitute a superior mechanical integrity with electro-conductive ohmic electrical characteristics even in a highly bent state. ZnO nanorods were grown in periodic arrays of circular bundles with varying inter-bundle distances in order to demonstrate a feasible device application.

## 2. Experimental details

The PET substrates were cleaned by sonication in isopropyl alcohol (IPA) (5 min) followed by ethanol (5 min). The substrates were blown dry with a stream of nitrogen gas. A thin layer (10 nm) of gold (Au) was then sputtered onto the PET substrates, followed by a ZnO seed layer of 6 nm *via* radio-frequency (RF) magnetron sputtering (Denton Vacuum Discovery 18 system) at room temperature. The purpose of the Au layer is to provide a conductive layer for the application of an electric field across the nanorods to induce the emission of electrons. However, it has been noted that the patterning and growth of nanorods on PET is also feasible without the Au layer. The thickness of the Au layer was kept to 10 nm so that it was thin enough to allow some degree of transparency of the device but still ensure good conductivity through the metal layer. The seeded substrates were then placed into a 25 ml growth solution containing 0.05 g of poly(ethyleneimine) solution (PEI), 25 mM of zinc nitrate hexahydrate and 25 mM of hexamethylenetetramine (HMT) in de-ionized (DI) water. The growth process was carried out at 90 °C for 3 h. A thin strip of Au at the edge of the PET substrate was left bare without any ZnO seed layer to allow good contact between the copper tape and the Au layer during the field emission measurements.

For patterned growth of ZnO nanorods on PET, the seeded substrates were first spincoated with AZ1518 photoresist and soft-baked on a hotplate at 100 °C for 60 s. The photoresist was then patterned with a laser of wavelength 405 nm and laser power of 66 mW. The pattern is a periodic array of circles (1  $\mu\text{m}$  in diameter) and a spacing of 2  $\mu\text{m}$  to 8  $\mu\text{m}$  between the adjacent circles. Development of the exposed photoresist was carried out in a diluted AZ developer (AZ 400 K developer: DI water = 1: 4) for 20 s, then rinsed in DI water and dried with a stream of compressed air. The patterned substrates were then placed in the same growth solution as mentioned above at 90 °C for 3 h. The fabrication steps are illustrated in the schematic diagram in Fig. 1.

Various characterization techniques were carried out on the samples. Scanning electron microscopy (SEM, JEOL FEG JSM 7001F) characterized the morphology of the synthesized products while the crystalline structure of the ZnO nanorods was analyzed using X-ray diffraction (XRD, Philips X-ray diffractometer equipped with graphite-monochromated Cu-K $\alpha$

radiation at  $\lambda = 1.541 \text{ \AA}$ ) and transmission electron microscopy (TEM, Phillips FEG CM300). Room temperature optical properties were measured by the UV-VIS-NIR spectrophotometer (UV-vis, Shimadzu UV-3600) and micro-photoluminescence (PL) with a He–Cd laser at 325 nm. The electrical properties of the samples were studied by current–voltage ( $I$ – $V$ ) measurements carried out using a Keithley 4200-SCS semiconductor characterization system. The field emission properties of the synthesized products were measured using a two-parallel-plate configuration in a vacuum chamber, with a base pressure of  $2 \times 10^{-6}$  Torr at room temperature. The sample was adhered to a Cu substrate cathode with double-sided copper tape while indium tin oxide (ITO) glass was used as the anode. The distance between the electrodes was kept at 70  $\mu\text{m}$  by a PET spacer with a circular hole of 0.28  $\text{cm}^2$ . A Keithley 237 high voltage source measurement unit (SMU) was used to apply a voltage of 0–1100 V between the two electrodes and to measure the emission current at the same time.

## 3. Results and discussion

The morphology of the synthesized ZnO nanorods on PET without patterning is shown in Fig. 2. The low (Fig. 2a) and high (Fig. 2b) magnification SEM images of the sample show dense, uniform growth across the entire substrate. The 30° tilted (Fig. 2c) and cross-sectional (Fig. 2d) views show well-aligned nanorods. The length of the nanorods is 2  $\mu\text{m}$  with an average diameter of 50 nm. Structural characterization of the hydrothermally grown nanorods was carried out *via* TEM. Fig. 2e shows that the nanorods have a uniform diameter with a smooth surface. The HRTEM image (Fig. 2f) shows lattice fringes with an interplanar spacing of  $\sim 0.52$  nm, confirming that the ZnO nanorods are single crystalline with a preferential growth in the [0001] direction. The corresponding selected area electron diffraction (SAED) pattern (inset of Fig. 2f) of the ZnO nanorod also implies that its growth is in the  $c$ -axis direction and suggests good crystallinity of the nanorod. XRD spectra of Au-coated PET (Au/PET) and ZnO nanorods grown on Au-coated PET (ZnO nanorods/Au/PET) were obtained and are shown in Fig. 3a. Both spectra have a very pronounced PET (100) peak at 26°. Other PET peaks present are the PET (12–2) at 46.6° and PET (2–30) at 52.9° as shown in the inset of Fig. 3a which shows a magnified view of the spectra in the range 30° to 60°. The only Au peak observed was the Au (111) peak at 38.2° which was found on both samples. The only peak that is present in the ZnO nanorods spectrum but not the Au/PET spectrum is the prominent ZnO (002) peak which can be well indexed to the hexagonal phase of ZnO with lattice constants  $a = 0.3242$  nm and  $c = 0.5194$  nm (JCPDS Card No. 79-0205). The (002) peak indicates preferential growth in the [0001] direction, and also good crystal structure and phase purity of the product.

Room temperature photoluminescence (PL) was carried out on ZnO nanorods synthesized on both Si and PET substrates (Fig. 3b) to study the optical properties. A Si substrate was included in this study to determine if the substrate affects the PL spectrum of the nanorods. A near band-edge emission peak at 380 nm and a broad yellow-orange emission band centered at 600 nm were observed in both samples. The yellow-orange emission defect peak observed in the spectra is most likely due to

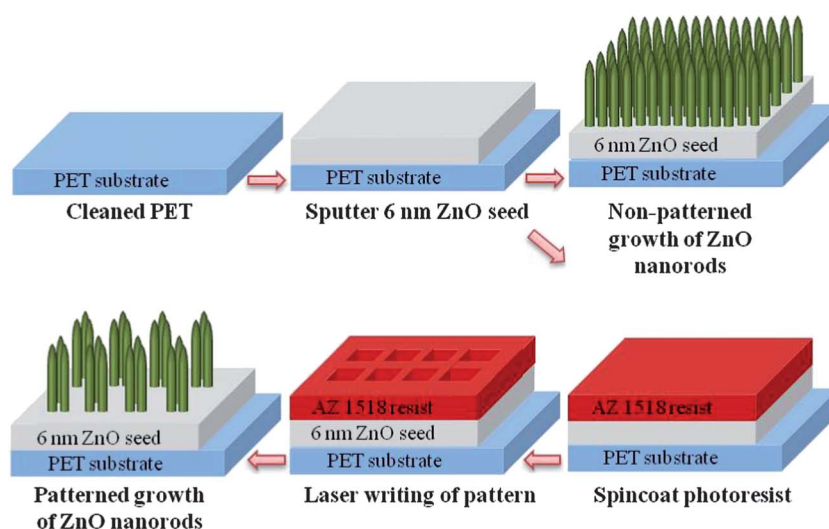


Fig. 1 The schematic approach of growing ZnO nanorods on PET substrate with and without patterning.

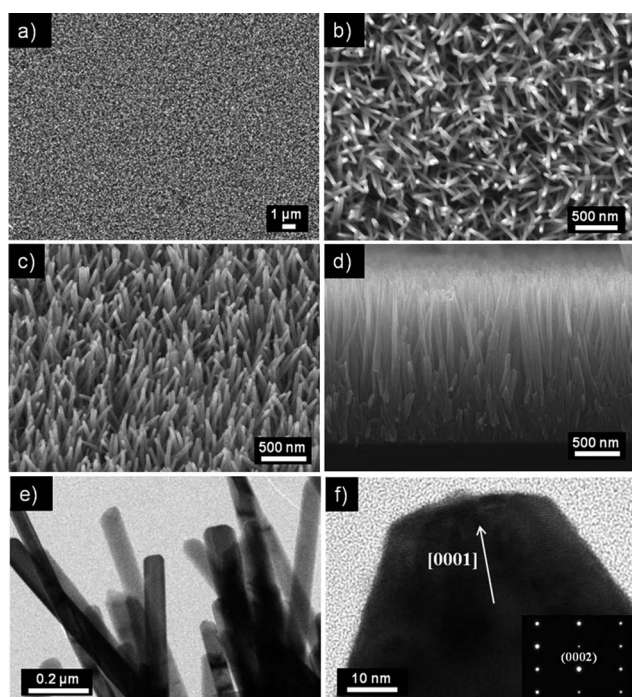
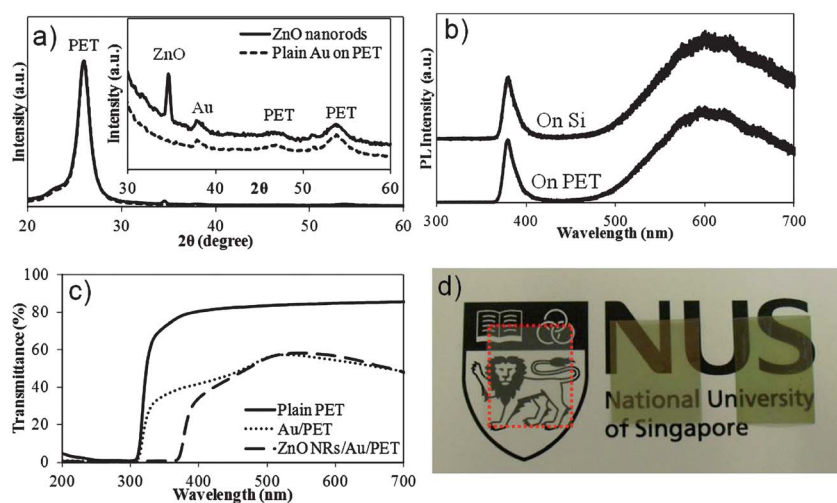


Fig. 2 (a) & (b) Low and high magnification SEM images of ZnO nanorods grown on a PET substrate. (c) 30° tilted view of ZnO nanorods. (d) Cross sectional view of ZnO nanorods. (e) TEM image of ZnO nanorods, and (f) HRTEM image of a nanorod showing the [0001] growth direction. The inset shows the corresponding selected area electron diffraction (SAED) pattern of the ZnO nanorod.

interstitial oxygen.<sup>11</sup> The intensities of the two peaks were noted to be similar for both samples. This similarity suggests that the optical properties of the ZnO nanorods grown on the PET substrate do not differ from those grown on rigid substrates such as Si. Room temperature UV-vis transmittance spectra of the samples were recorded by a UV-VIS-NIR spectrophotometer to determine the transparency of the synthesized products. Transmittance measurements were carried out on plain PET, PET

sputtered with 10 nm of Au (Au/PET) and ZnO nanorods grown on ZnO seeded Au/PET (ZnO nanorods/Au/PET). As shown in Fig. 3c, the transmittance of the plain PET is about 80–85% in the visible range (400 to 700 nm), and ultraviolet (UV) light of wavelength less than 306 nm is absorbed by the PET. After sputtering 10 nm of Au on the PET, the transmittance level in the visible range exhibited a peak value of 57% at 531 nm which decreased to 48% at 700 nm. The pronounced increase in absorption at longer wavelengths could be attributed to the surface plasmon resonance of the Au layer.<sup>12</sup> UV light of wavelength less than 306 nm was also absorbed due to the PET substrate. The spectrum of the sample after synthesis of ZnO nanorods exhibited a peak transmittance of 58% at 553 nm which was red-shifted from that of the Au/PET sample. The transmittance of wavelengths from 553 to 700 nm is quite similar to that of the Au/PET sample. However, the transmittance of UV light was red-shifted to 360 nm, instead of the 306 nm observed in the previous two samples. The absorption of UV light of 360 nm and less is due to the presence of the ZnO nanorods. A transmittance level of at least 40% in the visible range for the PET substrate with ZnO nanorods makes it viable as a semi-transparent flexible field emission device. An optical photograph illustrating the transparency of the samples is shown in Fig. 3d. The plain PET substrate (outlined in red) is placed on the extreme left, the Au/PET sample is placed in the center and the Au/PET with ZnO nanorods is positioned on the right. From the photograph, it can be seen that despite having a darker shade, the ZnO nanorods sample is fairly “see-through” or transparent.

Besides transparency, the mechanical and electrical integrity of the nanostructures on PET substrates is also of great concern. The homemade setup in Fig. 4a was used to bend the sample by various degrees of bending quantified by the angle  $\theta$ , as shown in Fig. 4a. From the SEM image (Fig. 4b inset), it can be observed that the film of ZnO nanorods grown on the PET substrate exhibits great flexibility and conforms to the bending of the substrate without any delamination of the nanorod film from the substrate. A series of SEM images (some not shown here) shows the state of the ZnO nanorods before and after cycling the



**Fig. 3** (a) XRD spectra of plain Au on PET and ZnO nanorods on Au-coated PET. (b) PL spectra of ZnO nanorods on Si and Au-coated PET substrates. (c) UV-vis transmittance spectrum and (d) photograph showing transparency of (from left to right): plain PET substrate (red-dotted outline), sputtered Au (10 nm) on PET and ZnO nanorods synthesized on Au/PET.

bending of the sample at  $\theta = 5^\circ$  and  $90^\circ$  100 times. The SEM images show that no cracks or delaminations were formed in the film of ZnO nanorods after bending it repeatedly many times. The excellent adhesion of the ZnO nanorods on the PET substrate under severe bending conditions suggests that the ZnO nanorods maintained mechanical robustness, thus making them suitable for flexible device applications.  $I$ - $V$  measurements of the sample were carried out at various stages of bending to determine if the bending affected the electrical characteristics of the ZnO nanorods. From the  $I$ - $V$  curves in Fig. 4c and 4d which show the results for compressive and tensile stress at  $\theta = 5^\circ$  respectively, it can be seen that the bending did not affect the ZnO nanorods.

There was a slight decrease in current during and after compressive bending and a slight increase in the current during and after tensile bending. This can be explained by the tighter packing of the ZnO nanorods during the tensile bending, resulting in more contacts within the nanorod network. When the bending is removed, conductivity falls and stabilises close to the original state. The structural and electrical characteristics integrity was maintained after the electromechanical testing.

Patterned growth of ZnO nanorods on PET was achieved via direct laser writing. The periodic array of  $1 \mu\text{m}$  circles with an array spacing of 2, 4, 6 and  $8 \mu\text{m}$  was created by laser writing on the ZnO seeded Au/PET substrate, spincoated with

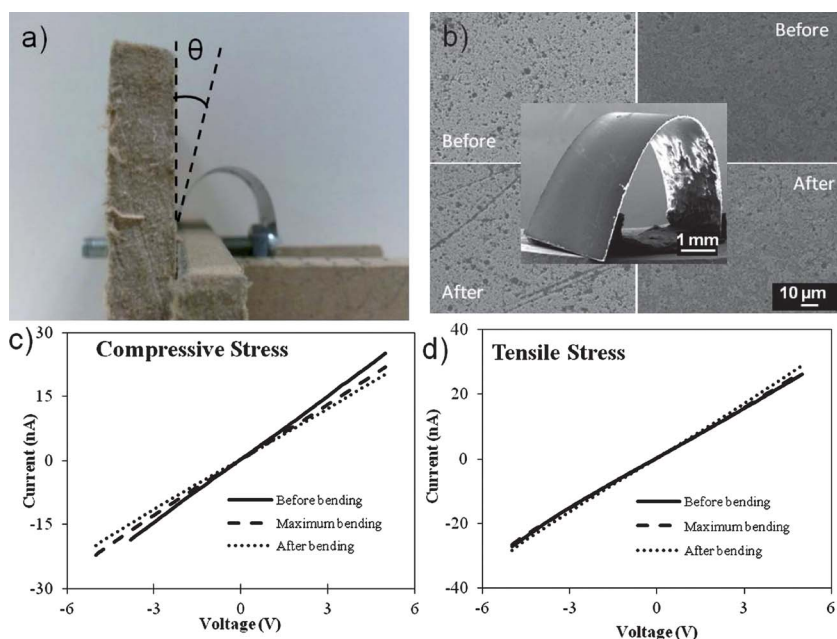


**Fig. 4** (a) Illustration of degree of bending. (b) SEM images of two areas on the sample before bending and after bending. Inset shows a bent flexible ZnO nanorods sample.  $I$ - $V$  curve of sample undergoing (c) compressive stress and (d) tensile stress. Maximum bending refers to  $\theta = 5^\circ$ .

a photoresist. Selective growth of ZnO nanorods was observed to occur only in the 1  $\mu\text{m}$  circles and no nanorods were found in the spaces in-between. Patterned growth of ZnO nanorods in array patterns with varying array spacing is shown in Fig. 5. The ZnO nanorods grew in bundles in the circles due to the disparity between the size of the circular pattern and the diameter of the nanorods. The size of the circle is 1  $\mu\text{m}$  while the diameter of the ZnO nanorods is between 80–600 nm. As a result, several nanorods could grow in the circle simultaneously, resulting in bundled growth of ZnO nanorods. The height of the nanorods (2–3.3  $\mu\text{m}$ ) is greater than the thickness of the photoresist (1–2  $\mu\text{m}$ ), and thus the growth direction of the nanorods is no longer confined to the circle once they grow past the photoresist. This caused some of the nanorods to grow at a tilted angle once they went above the photoresist, giving the bundles a flower-like appearance. The average diameter and height of the ZnO nanorods are detailed in Table 1 together with the corresponding array spacing. It was observed that as the array spacing increases, the diameter and height of the nanorods tend to increase. This is because as the array spacing increases, the number of nucleation sites on the substrate decreases, thus more reactants are available per nucleation site. As a result, the nanorods become larger in diameter and also grow taller.

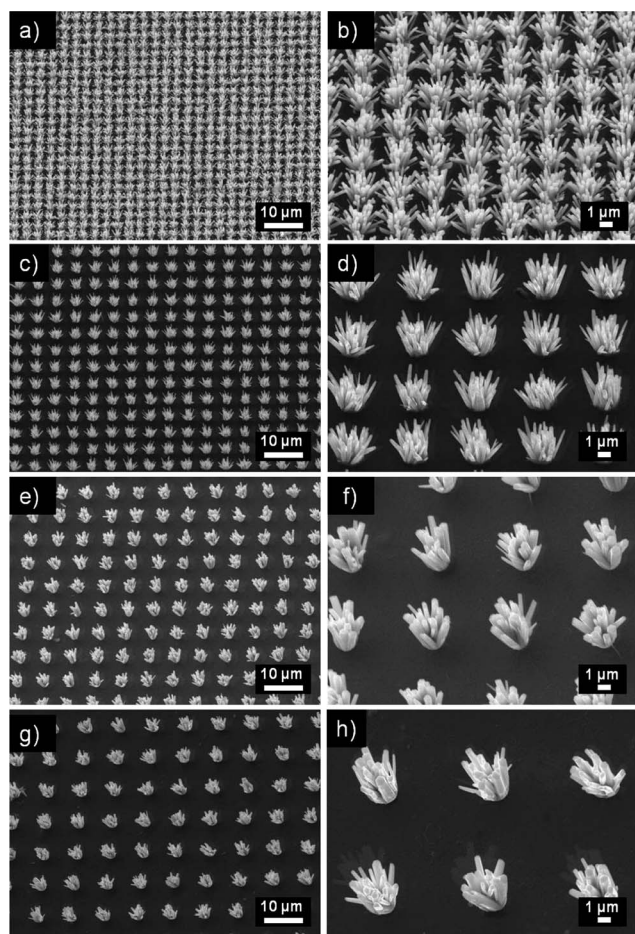


**Fig. 5** SEM images (30° tilted view) of magnification 1500 $\times$  and 5000 $\times$  for patterned growth with array spacing of (a, b) 2  $\mu\text{m}$ , (c, d) 4  $\mu\text{m}$ , (e, f) 6  $\mu\text{m}$ , and (g, h) 8  $\mu\text{m}$ .

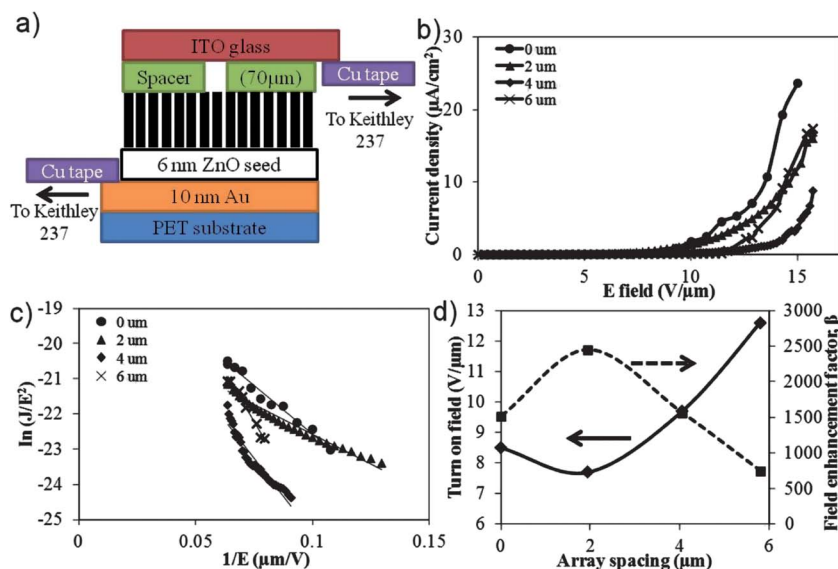
A practical device demonstration was carried out using the patterned ZnO nanorods on the PET substrate. The field emission characteristics are presented in Fig. 6 and Table 1. Fig. 6a shows the field emission measurement setup for the PET samples. A piece of indium tin oxide (ITO) glass was employed as the anode and the spacer used is a PET sheet of thickness 70  $\mu\text{m}$ . Strips of copper tape were pasted on the ITO surface of the anode and the Au layer of the cathode, which were subsequently connected to the Keithley 237 high voltage SMU. The plot of the emission current density  $J$  versus the applied field  $E$  from the samples is shown in Fig. 6b. The turn-on field ( $E_{\text{on}}$ ) is defined as the applied electric field required to produce an emission current density of 0.1  $\mu\text{A cm}^{-2}$ . The  $E_{\text{on}}$  of the ZnO nanorods grown on the non-patterned PET is 8.2  $\text{V } \mu\text{m}^{-1}$ . The emission current–voltage characteristics were analyzed using the Fowler–Nordheim ( $F-N$ ) equation:<sup>13</sup>

$$J = \frac{A\beta^2 E^2}{\phi} \exp\left(\frac{-B\phi^{3/2}}{\beta E}\right) \quad (1)$$

where  $J$  is the current density ( $\text{A cm}^{-2}$ ),  $E$  the applied field ( $\text{V } \mu\text{m}^{-1}$ ),  $\phi$  the work function of the field emitter (5.3 eV for ZnO),<sup>14</sup>  $\beta$  the field enhancement factor,  $A = 1.56 \times 10^{-10}$  ( $\text{A eV } \text{V}^{-2}$ ), and  $B = 6.83 \times 10^9$  ( $\text{V m}^{-1} \text{eV}^{-3/2}$ ). The dependency of the emission current density on the applied field, plotted as a  $\ln(J/E^2)$  versus  $1/E$  relationship is shown in Fig. 6c, where the slope of the fitted straight line corresponds to  $B\phi^{3/2}/\beta$ . This indicates that the field emission of the ZnO nanorods follows the  $F-N$  relationship,<sup>15</sup> and that the field emission mechanism is a barrier tunneling quantum mechanical process. From the  $F-N$  plots in Fig. 6c, the calculated field enhancement factor  $\beta$  for the non-patterned sample is 542. Despite the high aspect ratio of 80, the field emission property is poorer than that of the sample with 2  $\mu\text{m}$  array spacing. The 2  $\mu\text{m}$  sample has an aspect ratio of only 26 but produced an  $E_{\text{on}}$  of 5.7  $\text{V } \mu\text{m}^{-1}$  and  $\beta$  of 2449. The difference in field emission performance is due to the screening effect from the dense growth of nanorods.<sup>16</sup> Although the non-patterned sample has a high aspect ratio, the closely packed nanorods resulted in a much stronger screening effect between the emitters compared to the 2  $\mu\text{m}$  sample where the nanorods were spaced further apart. The sample with 4  $\mu\text{m}$  array spacing has an aspect ratio of 24, which is similar to the 2  $\mu\text{m}$  sample, but it shows a poorer field emission result with  $E_{\text{on}}$  of 7.7  $\text{V } \mu\text{m}^{-1}$  and  $\beta$  of 986. The larger array spacing can aid in further reduction of the screening effect, but it also results in much fewer emitters available for field emission, resulting in poorer field emission performance. The field emission performance deteriorates further for the 6 and 8  $\mu\text{m}$  array spacing samples due to the lower aspect ratio and decreasing number of emitters available on the samples. From Fig. 6d, it is observed that the sample with array spacing of 2  $\mu\text{m}$  produced the lowest turn-on field of 5.7  $\text{V } \mu\text{m}^{-1}$  and the highest field enhancement factor  $\beta$  of 2449 among the samples investigated. This can be attributed to the screening effect being at its weakest when the bundles are spaced 2  $\mu\text{m}$  apart. The spacing–height ratio is 0.8 for the 2  $\mu\text{m}$  sample, as shown in Table 1. Several papers investigating the screening effect of 1-dimensional (1D) field emitters such as ZnO<sup>17,18</sup> and carbon nanotubes (CNTs)<sup>19–21</sup> suggested that the ideal spacing–height ratio which gives the smallest screening effect is about 1–2.

**Table 1** Summary of nanorods' height and diameter, and field emission properties of non-patterned and patterned growth with various array spacing

Array spacing ( $\mu\text{m}$ )	Average height ( $\mu\text{m}$ )	Average diameter ( $\mu\text{m}$ )	Aspect ratio	$E_{\text{on}}$ ( $\text{V } \mu\text{m}^{-1}$ )	Calculated $\beta$	Spacing–height
0	2	0.05	80	8.5	1512	0
2	2.5	0.19	26	5.7	2449	0.8
4	2.7	0.22	24	7.7	986	1.5
6	3.1	0.55	11	9.1	742	1.9
8	3.3	0.66	10	Nil	Nil	2.3

**Fig. 6** (a) Schematic diagram of flexible field emitter device. (b)  $J$ – $E$  and (c)  $F$ – $N$  plots of the flexible field emitter. (d) Relationship between array spacing and turn-on field and  $\beta$ .

The trend observed in the field emission results of the samples with various array spacings shows that a spacing–height ratio of 0.8 (2  $\mu\text{m}$  spacing sample) is ideal for minimal screening effect and gives the best field emission properties. This value of 0.8 is lower than the 1–2 reported in the literature. However, it was also observed that the field emission result shows some degradation when the spacing–height ratio is increased to 1.5 (4  $\mu\text{m}$  spacing sample). This suggests that a better field emission performance could be obtained if the spacing–height ratio was adjusted to a value between 0.8 and 1.5.

#### 4. Conclusions

We have successfully demonstrated laser writing lithography patterns on transparent flexible PET. Furthermore, practical device demonstration of field emission applications was also presented. The optically transparent nanorods on the PET platform exhibited superior structural integrity with ohmic electro-conduction in a bent state. The feasibility of optically transparent and mechanically flexible electronic devices could open the door to next-generation ‘see-through’, shock-proof and conformable display technologies.

#### Acknowledgements

This work is supported by the National University of Singapore (NUS) grant R-263-000-532-112 and R-263-000-653-731.

#### References

- S. Ju, A. Facchetti, Y. Xuan, J. Liu, F. Ishikawa, F. Ye, C. Zhou, T. J. Marks and D. B. Janes, *Nat. Nanotechnol.*, 2007, **2**, 378.
- S. Kwon, W. Hong, G. Jo, J. Maeng, T. Kim, S. Song and T. Lee, *Adv. Mater.*, 2008, **20**, 4557.
- M. S. Oh, W. Choi, K. Lee, D. K. Hwang and S. Im, *Appl. Phys. Lett.*, 2008, **93**, 033510.
- L. Vayssieres, *Adv. Mater.*, 2003, **15**, 464.
- J. Qiu, X. Li, W. He, S. J. Park, H. K. Kim, Y. H. Hwang, J. H. Lee and Y. D. Kim, *Nanotechnology*, 2009, **20**, 155603.
- M. Kevin, Y. H. Fou, A. S. W. Wong and G. W. Ho, *Nanotechnology*, 2010, **21**, 315602.
- M. Law, L. E. Greene, J. C. Johnson, R. Saykally and P. D. Yang, *Nat. Mater.*, 2005, **4**, 455.
- H. W. Kang, J. H. Lee, J. Yeo, Y. S. Rho, J. O. Hwang, S. O. Kim, S. Hong, S. H. Ko, P. Lee, S. Y. Han and H. J. Sung, *J. Phys. Chem. C*, 2011, **115**, 11435.
- C. H. Wang, A. S. W. Wong and G. W. Ho, *Langmuir*, 2007, **23**, 11960.
- M. G. Kang and L. J. Guo, *J. Vac. Sci. Technol. B*, 2007, **25**, 2637.
- D. Li, Y. H. Djuricic, A. B. Leung, Z. T. Liu, M. H. Xie, S. L. Shi, S. J. Xu and W. K. Chan, *Appl. Phys. Lett.*, 2004, **85**, 1601.
- J. Siegel, O. Lyutakov, V. Rybka, Z. Kolská and V. Švorčík, *Nanoscale Res. Lett.*, 2011, **6**, 96.
- W. L. Hughes and Z. L. Wang, *Appl. Phys. Lett.*, 2005, **86**, 043106.
- T. Minami, T. Miyata and T. Yamamoto, *Surf. Coat. Technol.*, 1998, **108**, 583.
- Q. Zhao, H. Z. Zhang, Y. W. Zhu, S. Q. Feng, X. C. Sun, J. Xu and D. P. Yu, *Appl. Phys. Lett.*, 2005, **86**, 203115.

- 16 X. M. Qian, H. B. Liu, Y. B. Guo, Y. L. Song and Y. L. Li, *Nanoscale Res. Lett.*, 2008, **3**, 303.
- 17 J. H. Lee, Y. W. Chung, M. H. Hon and I. C. Leu, *Appl. Phys. A*, 2009, **97**, 403.
- 18 C. Li, Y. Yang, X. W. Sun, W. Lei, X. B. Zhang, B. P. Wang, J. X. Wang, B. K. Tay, J. D. Ye, G. Q. Lo and D. L. Kwong, *Nanotechnology*, 2007, **18**, 135604.
- 19 J. M. Bonard, N. Weiss, H. Kind, T. Stöckli, L. Forró, K. Kern and A. Châtelain, *Adv. Mater.*, 2001, **13**, 184.
- 20 L. Nilsson, O. Groening, C. Emmenegger, O. Kuettel, E. Schaller, L. Schlapbach, H. Kind, J. M. Bonard and K. Kern, *Appl. Phys. Lett.*, 2000, **76**, 2071.
- 21 J. S. Suh, K. S. Jeong, J. S. Lee and I. Han, *Appl. Phys. Lett.*, 2002, **80**, 2392.